Comput. Methods Appl. Mech. Engrg. 217–220 (2012) 46–57

Contents lists available at SciVerse ScienceDirect

Comput. Methods Appl. Mech. Engrg.

journal homepage: www.elsevier.com/locate/cma

# A 3D interface-enriched generalized finite element method for weakly discontinuous problems with complex internal geometries

Soheil Soghrati [a], Philippe H. Geubelle [b,*]

[a] Department of Civil and Environmental Engineering, University of Illinois at Urbana-Champaign, 205 North Mathews Avenue, Urbana, IL 61801, USA
[b] Department of Aerospace Engineering, University of Illinois at Urbana-Champaign, 104 South Wright Street, Urbana, IL 61801, USA

ARTICLE INFO

*Article history:*
Received 24 July 2011
Received in revised form 14 November 2011
Accepted 27 December 2011
Available online 4 January 2012

*Keywords:*
GFEM/XFEM
Weak discontinuity
Convection–diffusion equation
Heat transfer problem
Convergence study
Heterogeneous materials

ABSTRACT

An interface-enriched generalized finite element method (GFEM) is introduced for 3D problems with discontinuous gradient fields. The proposed method differs from conventional GFEM by assigning the generalized degrees of freedom to the interface nodes, i.e., nodes generated along the interface when creating integration subdomains, instead of the nodes of the original mesh. A linear combination of the Lagrangian shape functions in these integration subelements are then used as the enrichment functions to capture the discontinuity in the gradient field. This approach provides a great flexibility for evaluating the enrichment functions, including for cases where elements are intersected with multiple interfaces. We show that the method achieves optimal rate of convergence with meshes which do not conform to the phase interfaces at a computational cost similar to or lower than that of conventional GFEM. The potential of the method is demonstrated by solving several heat transfer problems with discontinuous gradient field encountered in particulate and fiber-reinforced composites and in actively-cooled microvascular materials.

© 2012 Elsevier B.V. All rights reserved.

## 1. Introduction

The generalized/extended finite element methods (GFEM/XFEM), first introduced in [1–4], is now widely used by the computational mechanics community to solve problems with strong or weak discontinuities, i.e., problems presenting discontinuities in the solution or gradient fields, respectively. By eliminating the need for meshes that conform to the internal geometry of the problem and/or propagating discontinuities independently of the finite element discretization, these methods provide a level of flexibility absent in standard finite element methods (FEM). This unique capability is achieved by incorporating a priori information on the solution field in the numerical approximation with the aid of enrichment functions. For problems with weak or strong discontinuities, appropriate enrichment functions are selected to capture the jump in the gradient or solution fields, respectively, allowing for meshes that are independent of the morphology of the problem. Application areas of the GFEM/XFEM include fracture mechanics [5–10], multiscale modeling [11], contact problems [12,13], solidification [14], modeling of dislocations [15,16], and phase interfaces [17–19]. A comprehensive review of the GFEM/XFEM method, the associated enrichment functions, and their implementation issues is provided in [20].

In the current paper, we present an *interface-enriched generalized finite element method* (IGFEM) for 3D problems with $C^0$-continuous fields such as those encountered in thermal and structural problems involving composites [21–23], polycrystalline materials [24,25], fluid/solid interaction [26], and conjugate problems with multiple phases [27]. Unlike in conventional GFEM where the generalized degrees of freedom (dofs) are assigned to the nodes of the original mesh, the IGFEM assigns the generalized dofs to interface nodes created by the intersection of the phase interface with the non-conforming mesh. Armero and co-workers [28] have proposed the introduction of element-based interface enrichments for strongly discontinuous problems where the generalized dofs are associated with the elements themselves. However, the approach adopted in the present work relies on the enrichment of the interface nodes and thereby enforcing continuity of the enriched solution between adjacent elements.

A unique feature of the IGFEM is the evaluation of the enrichment functions, which are obtained through a linear combination of the standard Lagrangian shape functions of the integration elements. Hence, regardless of the orientation and number of interfaces intersecting with the edges of an element, the IGFEM provides a simple approach to construct the enrichment functions and can be considered as an *h-hierarchical* method [29]. In this work, we present a strategy for creating the integration elements and the corresponding enrichment functions for tetrahedral elements. The formulation of the IGFEM for 2D problems has been

* Corresponding author. Tel.: +1 217 244 7648; fax: +1 217 244 0720.
*E-mail address:* geubelle@illinois.edu (P.H. Geubelle).

0045-7825/$ - see front matter © 2012 Elsevier B.V. All rights reserved.
doi:10.1016/j.cma.2011.12.010

# Report Documentation Page

*Form Approved*
*OMB No. 0704-0188*

Public reporting burden for the collection of information is estimated to average 1 hour per response, including the time for reviewing instructions, searching existing data sources, gathering and maintaining the data needed, and completing and reviewing the collection of information. Send comments regarding this burden estimate or any other aspect of this collection of information, including suggestions for reducing this burden, to Washington Headquarters Services, Directorate for Information Operations and Reports, 1215 Jefferson Davis Highway, Suite 1204, Arlington VA 22202-4302. Respondents should be aware that notwithstanding any other provision of law, no person shall be subject to a penalty for failing to comply with a collection of information if it does not display a currently valid OMB control number.

| | | |
|---|---|---|
| 1. REPORT DATE<br>**2012** | 2. REPORT TYPE | 3. DATES COVERED<br>**00-00-2012 to 00-00-2012** |
| 4. TITLE AND SUBTITLE<br>**A 3D interface-enriched generalized finite element method for weakly discontinuous problems with complex internal geometries** | | 5a. CONTRACT NUMBER<br>5b. GRANT NUMBER<br>5c. PROGRAM ELEMENT NUMBER |
| 6. AUTHOR(S) | | 5d. PROJECT NUMBER<br>5e. TASK NUMBER<br>5f. WORK UNIT NUMBER |
| 7. PERFORMING ORGANIZATION NAME(S) AND ADDRESS(ES)<br>**University of Illinois at Urbana-Champaign,Department of Civil and Environmental Engineering,205 North Mathews Avenue,Urbana,IL,91801** | | 8. PERFORMING ORGANIZATION REPORT NUMBER |
| 9. SPONSORING/MONITORING AGENCY NAME(S) AND ADDRESS(ES) | | 10. SPONSOR/MONITOR'S ACRONYM(S)<br>11. SPONSOR/MONITOR'S REPORT NUMBER(S) |

12. DISTRIBUTION/AVAILABILITY STATEMENT
**Approved for public release; distribution unlimited**

13. SUPPLEMENTARY NOTES

14. ABSTRACT
**An interface-enriched generalized finite element method (GFEM) is introduced for 3D problems with discontinuous gradient fields. The proposed method differs from conventional GFEM by assigning the generalized degrees of freedom to the interface nodes, i.e., nodes generated along the interface when creating integration subdomains, instead of the nodes of the original mesh. A linear combination of the Lagrangian shape functions in these integration subelements are then used as the enrichment functions to capture the discontinuity in the gradient field. This approach provides a great flexibility for evaluating the enrichment functions, including for cases where elements are intersected with multiple interfaces. We show that the method achieves optimal rate of convergence with meshes which do not conform to the phase interfaces at a computational cost similar to or lower than that of conventional GFEM. The potential of the method is demonstrated by solving several heat transfer problems with discontinuous gradient field encountered in particulate and fiber-reinforced composites and in actively-cooled microvascular materials.**

15. SUBJECT TERMS

| 16. SECURITY CLASSIFICATION OF: | | | 17. LIMITATION OF ABSTRACT | 18. NUMBER OF PAGES | 19a. NAME OF RESPONSIBLE PERSON |
|---|---|---|---|---|---|
| a. REPORT<br>**unclassified** | b. ABSTRACT<br>**unclassified** | c. THIS PAGE<br>**unclassified** | **Same as Report (SAR)** | **12** | |

previously presented in [30], together with a convergence study and a detailed comparison of the this method with conventional GFEM. In the current work, besides extending the IGFEM formulation to 3D problems, we put more emphasis on how the IGFEM handles geometrical complexities involved in these problems and study the application of this method for solving several engineering problems with intricate internal geometries.

The outline of this paper is as follows: In the next section, we present the strong and weak forms of the convection–diffusion equation describing the thermal response of actively cooled microvascular composites that motivated this work. It should be noted, however, that although the thermal convection–diffusion equation is the focus of this work, the IGFEM can readily extended for other problems, including those characterized by strong discontinuities as briefly discussed later in the manuscript. In the remainder of that section, we review some of the key features of conventional GFEM approximations before introducing the 3D IGFEM formulation based on a discretization with tetrahedral elements. A short discussion is also provided in that section to compare the computational cost of the 3D IGFEM with that of conventional GFEM. We then analyze in Section 3 the performance of the IGFEM by performing a detailed convergence study with non-conforming meshes and comparing the results with those of the standard FEM based on matching meshes. Finally, we present in Section 4 the IGFEM solution to several heat transfer problems with weak discontinuities to illustrate the capabilities of the method to handle thermal problems with a variety of intricate internal geometries.

## 2. Convection–diffusion equation and GFEM/IGFEM formulations

Consider the open domain $\Omega = \Omega_s \cup \Omega_f \subset \mathbb{R}^3$ and its closure $\overline{\Omega}$. The domain is partitioned into two separate regions $\Omega_s$ and $\Omega_f$ corresponding to solid and fluid phases, respectively. A velocity field $\mathbf{v} : \Omega \to \mathbb{R}^3$ is then defined for the convective term, with $\mathbf{v} = 0$ in $\Omega_s$ where only conduction contributes to the heat transfer. The boundary $\Gamma = \overline{\Omega} - \Omega$ with the outward unit normal vector $\mathbf{n}$ has been divided into three mutually exclusive partitions $\Gamma_u$, $\Gamma_q$, and $\Gamma_h$. Here, $\Gamma_u$ corresponds to Dirichlet boundary conditions with the prescribed temperature $\bar{u} : \Gamma_u \to \mathbb{R}, \Gamma_q$ corresponds to Neumann boundary conditions with the heat flux $q : \Gamma_q \to \mathbb{R}$, and $\Gamma_h$ represents the region with Robin (convective) boundary conditions with the heat transfer coefficient $h : \Gamma_h \to \mathbb{R}$, and ambient temperature $u_\infty : \Gamma_h \to \mathbb{R}$. Assuming the thermal conductivity $\boldsymbol{\kappa} : \overline{\Omega} \to \mathbb{R}^3 \times \mathbb{R}^3$, density $\rho : \Omega \to \mathbb{R}$, and specific heat $c_p : \Omega \to \mathbb{R}$ as the material properties of the domain and given the heat source $f : \Omega \to \mathbb{R}$, the strong form of the convection–diffusion equations is then expressed as: find $u : \overline{\Omega} \to \mathbb{R}$ such that:

$$\begin{aligned} &-\nabla \cdot (\boldsymbol{\kappa}\nabla u) + \rho c_p \mathbf{v} \cdot \nabla u = f \quad \text{on } \Omega, \\ &u = \bar{u} \quad \text{on } \Gamma_u, \\ &\boldsymbol{\kappa}\nabla u \cdot \mathbf{n} = q \quad \text{on } \Gamma_q, \\ &\boldsymbol{\kappa}\nabla u \cdot \mathbf{n} = h(u_\infty - u) \quad \text{on } \Gamma_h. \end{aligned} \tag{1}$$

The weak form of (1) is expressed as follows: assuming the solution field to belong to the function space $\mathcal{U}$ such that $\mathcal{U} = \{u : u|_{\Gamma_u} = \bar{u}\} \subset H^1(\overline{\Omega})$ and given the function space $\mathcal{W} = \{w : w|_{\Gamma_u} = 0\} \subset H^1(\overline{\Omega})$ as the space of the weight functions, find $u \in \mathcal{U}$ such that for all $w \in \mathcal{W}$:

$$\begin{aligned} &\int_\Omega \nabla w \cdot (\boldsymbol{\kappa}\nabla u)\, d\Omega + \int_{\Omega_f} \rho c_p w \mathbf{v} \cdot \nabla u\, d\Omega + \int_{\Gamma_h} hwu\, d\Gamma_h \\ &= \int_\Omega wf\, d\Omega + \int_{\Gamma_q} wq\, d\Gamma_q, + \int_{\Gamma_h} hwu_\infty\, d\Gamma_h. \end{aligned} \tag{2}$$

### 2.1. Conventional GFEM formulation

The GFEM formulation is based on the Galerkin method where $\mathcal{U}^h \subset \mathcal{U}$ and $\mathcal{V}^h \subset \mathcal{V}$ are selected such that $\mathcal{U}^h = \mathcal{V}^h$. The domain $\Omega$ is then discretized into $M$ finite elements, $\Omega \cong \Omega^h \equiv \cup_{i=1}^m \overline{\Omega}_i$, which do not need to conform to the phase interfaces in $\Omega$. The standard Lagrangian shape functions, $\{N_i(\mathbf{x}) : \mathbf{x} \to \mathbb{R}\}_{i=1}^n$, are used to approximate the solution field (and thus the weight functions) in elements not cut by any interface, where $n$ is the number of nodes in each element. To retrieve the missing information in the solution field in elements located over the interface, a set of $m$ enrichment functions at each node of the element, $\{\varphi_{ij}(\mathbf{x}) : \mathbf{x} \to \mathbb{R}\}_{i,j=1}^{n,m}$, is employed to evaluate the gradient discontinuity. The GFEM approximation of the solution field for (2) is then expressed as:

$$u^h(\mathbf{x}) = \sum_{i=1}^n N_i(\mathbf{x})\bar{u}_i + \sum_{i=1}^n N_i(\mathbf{x}) \sum_{j=1}^m \varphi_{ij}(\mathbf{x})\tilde{u}_{ij}. \tag{3}$$

The first term in (3) represents the standard FEM part of the approximation although $\bar{u}_i$ may not represent the nodal values of the solution if the enrichment functions $\varphi_{ij}$ do not vanish at the nodes. The second term, i.e., the contribution of the enrichment functions to the solution field, uses the concept of the *partition of unity* $\left(\sum_{i=1}^n N_i(\mathbf{x}) = 1\right)$ to localize the effect of enrichment functions in each element and provide a uniform enrichment along the interface. It must be noted that, for certain enrichment functions, the enriched nodes might be extended to elements adjacent to those intersected by the interface, known as blending elements, to maintain optimal rate of convergence [31]. This correction is required since the partition of unity is unable to reproduce fully the enrichment functions in the blending elements and thus corrective enrichment functions are employed to create a smooth transition between standard FEM elements and those cut by the interface.

Although the implementation of the GFEM is very similar to that of the standard FEM, two GFEM-related implementation issues need to be addressed. The first one is the quadrature in the enriched elements due to weak or strong discontinuities in the enrichment functions. The most common approach to achieve an accurate quadrature in these elements consists in dividing them into subdomains, referred to as integration sub-elements, with edges that conform to the phase interfaces passing through the element [5,6]. The aspect ratio of these integration elements does not affect the accuracy of the solution as they only serve as subdomains for choosing appropriate integration points. The second issue appears at enriched nodes located over the boundaries with Dirichlet boundary conditions, i.e., prescribed values of the temperature in the current work. Since the solution field at each node is obtained from the contribution of both the standard and generalized dofs, and since the enrichment functions do not necessarily disappear at the boundary nodes, the prescribed field values cannot be directly assigned at such nodes. In this case, other approaches such as Lagrange multipliers or penalty method must be employed to enforce the prescribed values of the solution field at enriched nodes [32,33].

### 2.2. IGFEM formulation

The major difference between the IGFEM and conventional GFEM consists in relocating the generalized dofs from nodes of the original mesh to those of integration sub-elements located over the interface, referred to as *interface nodes*. We then assign an enrichment function to each interface node, remove the partition of unity from the evaluation of the enrichment functions, and express the IGFEM approximation as:

$$u^h(\mathbf{x}) = \sum_{i=1}^{n} N_i(\mathbf{x})\bar{u}_i + \sum_{i=1}^{k} s\psi_i(\mathbf{x})\hat{u}_i^{int}. \tag{4}$$

As before, the first term in (4) corresponds to the standard FEM portion of the approximation. Since the generalized dofs are attached to the interface nodes, the standard dofs in this first term always represent the field values at the nodes of the original mesh. The second term in (4) is the contribution of the enrichment functions in approximating the solution field along the phase interface where $\hat{u}_i^{int}$ are the generalized dofs. The enrichment functions in IGFEM, i.e., $\{\psi_i(\mathbf{x}) : \mathbf{x} \to \mathbb{R}\}_{i=1}^{n}$, must capture the gradient jump in the solution field inside an element while vanishing at the nodes and edges of that element which are not cut by the interface. The latter condition for the enrichment functions is necessary to avoid discontinuities alongs the edges of the enriched elements and adjacent elements, i.e., to ensure the conformity of the approximate field along the boundary of the elements, and thus avoid any corrections for blending elements. As explained below, the parameter $s$ is a scaling factor used to avoid sharp gradients in the enrichment functions.

In this work, we describe the evaluation of the enrichment functions for tetrahedral elements, although the approach can be readily extended to other types of elements. Fig. 1 illustrates four different scenarios by which a four-node tetrahedral element may be cut by an interface and the associated division of the element into integration subdomains. The approach adopted here consists in creating the *minimum* number of integration elements for accurate quadrature over the parent (original) element to facilitate the evaluation of enrichment functions. A tetrahedral element is then divided into a combination of tetrahedral and pentahedral (wedge) elements based on the orientation of the interface with respect to the element edges. To capture the gradient discontinuity along the interface, the enrichment functions corresponding to Fig. 1(a)–(d) are expressed as:

$$\begin{aligned}
&(a)\ \psi_1 = N_1^{(1)} + N_1^{(2)}, \quad \psi_2 = N_2^{(1)} + N_4^{(2)}, \quad \psi_3 = N_4^{(1)} + N_2^{(2)}, \\
&\quad \psi_4 = N_5^{(1)} + N_5^{(2)}, \\
&(b)\ \psi_1 = N_1^{(1)} + N_4^{(2)}, \quad \psi_2 = N_2^{(1)} + N_5^{(2)}, \quad \psi_3 = N_3^{(1)} + N_6^{(2)}, \\
&(c)\ \psi_1 = N_1^{(1)} + N_1^{(2)}, \quad \psi_2 = N_2^{(1)} + N_2^{(2)} + N_1^{(3)}, \\
&(d)\ \psi_1 = N_1^{(1)} + N_1^{(2)},
\end{aligned} \tag{5}$$

respectively. Please note that the creation of wedge element in the IGFEM is not required and that a parent element can be discretized using tetrahedral elements only, for which the enrichment functions are constructed differently based on the number of integration sub-elements.

A possible issue with the aforementioned approach for evaluating the enrichment functions may occur when integration elements with very high aspect ratios are created, i.e., when the interface intersecting the tetrahedral elements happens to be very close to one of the nodes of the original mesh. Since the Lagrangian shape functions of these sub-elements contribute to the evaluation of the enrichment functions in the parent element, the high aspect ratio leads to high gradient values and thereby to an ill-conditioned stiffness matrix. To address this issue, we employ a scaling factor $s$ as introduced in (4) to avoid excessively large gradients in the enrichment functions [19]. To evaluate this parameter, we adopt the approach suggested in [30] and define $s$ as:

$$s = \left(\frac{2\min(x_1, x_2)}{x_1 + x_2}\right)^2, \tag{6}$$

where $x_1$ and $x_1$ are shown in Fig. 2.

Eq. (6) represent a parabolic function defined over the edge of the parent element holding an interface node, with zero value at the defining nodes of this edge and unity in the middle of it. As the interface approaches one of the nodes of the element, the scaled enrichment function goes to zero and vanishes when the interface coincides with an FEM node. It must be emphasized that the scaling factor $s$ has a constant value in an element cut by the interface and the quadratic function introduced in (6) has only been implemented to evaluate this value.

A key advantage of the IGFEM is its ability to handle problems with complex geometries or microstructures by creating enrichment functions for special cases. Ref. [30] describes the evaluation of enrichment functions for the case where two or more interfaces intersect inside an element for 2D problems. This is achieved by creating integration elements that conform to the geometry of the intersecting interfaces inside the parent element and using the linear interpolation of the corresponding Lagrangian

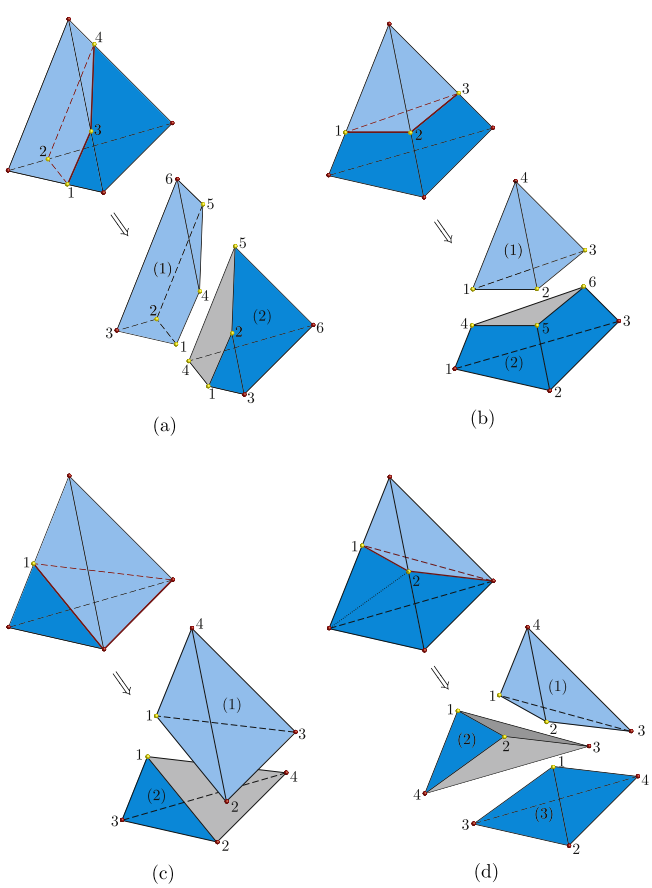


**Fig. 1.** Evaluation of enrichment functions for the 3D IGFEM: four scenarios of creating the integration subdomains composed of tetrahedral and wedge elements, and the corresponding numbering of integration elements used to evaluate the enrichment functions.

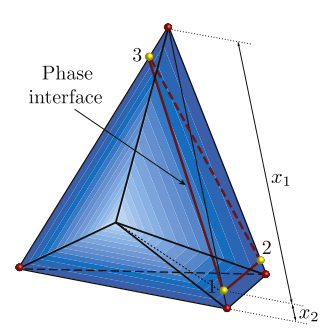


**Fig. 2.** Geometrical parameters $x_1$ and $x_1$used in the scaling factor entering the enrichment function associated with interface node 1 (Eq. (6)).

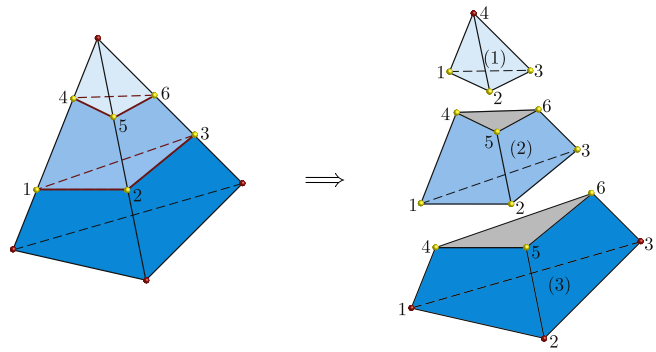


**Fig. 3.** Creation of integration elements for the evaluation of the enrichment functions in the IGFEM for an element cut by two interfaces.

shape functions as the enrichment functions. The same approach can be extended to 3D problems where a combination of tetrahedral and wedge integration elements that conform to the phase interfaces are used to discretize the parent element and evaluate the associated enrichment functions. Similarly, the IGFEM provides the framework for the evaluation of enrichment functions for more complex cases, where most conventional GFEM formulations tend to fail, such as cases where elements are intersected by multiple interfaces. Fig. 3 shows one of the possible scenarios of a four-node tetrahedral element cut by two interfaces and the corresponding integration elements created to evaluate the enrichment functions, which are obtained as:

$$\psi_1 = N_1^{(2)} + N_4^{(3)}, \quad \psi_2 = N_2^{(2)} + N_5^{(3)}, \quad \psi_3 = N_3^{(2)} + N_6^{(3)},$$
$$\psi_4 = N_1^{(1)} + N_4^{(2)}, \quad \psi_5 = N_2^{(1)} + N_5^{(2)}, \quad \psi_6 = N_3^{(1)} + N_6^{(2)}. \tag{7}$$

The enrichment function for other orientations of the element with respect to the phase interfaces can be evaluated similarly.

Many of the comments made in [30] to compare the 2D implementation of the GFEM and IGFEM apply to the 3D case discussed here. For instance, enforcing the Dirichlet boundary conditions in the IGFEM is similar to that of the standard FEM at the nodes of the elements intersected by the interface because the generalized dofs are moved to the interface nodes. Also, the computational cost of the 3D IGFEM with tetrahedral elements compares favorably with that of the conventional GFEM, especially for cases where blending elements are introduced. It can be shown that the number of generalized dofs introduced at the interface nodes in the IGFEM is equal to that of conventional GFEM with no correction in the blinding elements. Moreover, considerably more generalized dofs are added in conventional GFEM if enriching all the nodes of the blending elements is necessary for achieving the optimal rate of convergence. In other words, the cost of the numerical solution via IGFEM for 3D problems is equal to that of the best case of conventional GFEM.

Finally, although we only address in the current work problems with weak discontinuities, constructing the enrichment functions for problems with strong discontinuities within the IGFEM framework is straightforward. The enrichment functions needed for this class of problems can simply be obtained by switching the sign used in the linear combination of the Lagrangian functions in (5). For instance, the enrichment functions associated with the integration elements shown in Fig. 1 for problems with strong discontinuities can be written as:

$$\psi_1 = N_1^{(1)} - N_4^{(2)}, \quad \psi_2 = N_2^{(1)} - N_5^{(2)}, \quad \psi_3 = N_3^{(1)} - N_6^{(2)}. \tag{8}$$

The opposite signs of the Lagrangian shape functions in each integration element used for evaluating the enrichment functions in (8) can then simulate the discontinuity in the solution field along the interface.

## 3. Convergence study

Two example problems are presented in this section to study the convergence rates of the 3D IGFEM. In these examples, we use as reference solution either a closed-form solution or the solution obtained with the standard FEM with a highly refined conforming mesh. The IGFEM results obtained with non-conforming meshes are then compared with those provided by the standard

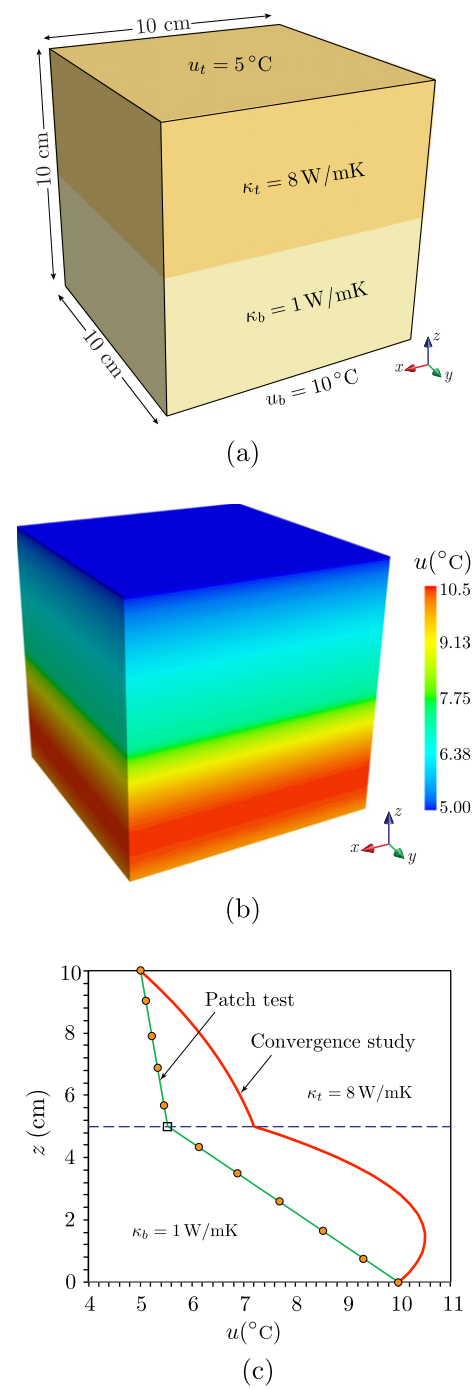


**Fig. 4.** (a) Problem description, and (b) GFEM solution for the first example problem. (c) Temperature profile along the $z$-axis obtained with the IGFEM solver for both the convergence study and the patch test.

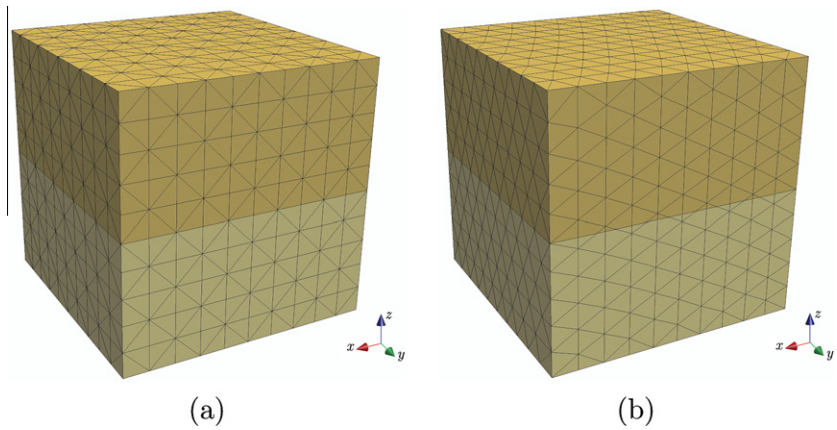


**Fig. 5.** (a) Structured conforming mesh used for the standard FEM solution, and (b) unstructured non-conforming mesh used for the IGFEM solution of the first example problem investigated in the convergence study.

FEM with conforming meshes with the same level of refinement to verify the optimal rate of convergence. We provide the convergence results in the $L_2$- and $H^1$-norm of the error, expressed as:

$$\|e\|_{L_2(\Omega)} = \|u - u^h\|_{L_2(\Omega)} = \sqrt{\int_\Omega (u-u^h)^2 d\Omega},$$
$$\|e\|_{H^1(\Omega)} = \|u - u^h\|_{H^1(\Omega)} = \sqrt{\int_\Omega (u-u^h)^2 + \int_\Omega \|\nabla u - \nabla u^h\|^2 d\Omega}. \tag{9}$$

### 3.1. Example 1: Constant gradient jump over a flat interface

The dimensions and boundary conditions of the first example problem are presented in Fig. 4. The cubic domain is composed of two regions along the $z$-axis with conductivity values of 1 and 8 W/m K for the lower and upper sections, respectively. The boundary conditions for this problem are prescribed temperatures 5 and 10 °C along the top and bottom surfaces, respectively, while the other surfaces are insulated. With the origin of the Cartesian coordinates system located at the lower front corner of the cubic domain, a distributed heat source $f(x,y,z) = 5000(z^2 - z + 1)$ is applied, yielding the following exact temperature field in the domain:

$$u(x,y,z) = \begin{cases} -33750z^4 + 833.3z^3 - 2500z^2 + 70.9z + 10 & \text{if } z < 0.05 \\ -4218.7z^4 + 104.2z^3 - 312.5z^2 + 8.86z + 7.56 & \text{if } z \geqslant 0.05. \end{cases} \tag{10}$$

Fig. 4 illustrates the IGFEM solution field for this problem with a nonconforming mesh built over a $16 \times 16 \times 16$ grid. As expected, the thermal conductivity mismatch generates a jump in the gradient field at $z$ = 5 cm. This gradient discontinuity is accurately captured by the IGFEM as shown in Fig. 4, which depicts the temperature profile along the $z$-axis.

Before the convergence study, we present a modified patch test by removing the heat source applied over the domain and showing how the IGFEM can capture the gradient discontinuity along the interface. The exact solution for this problem is a linear variation of the temperature along the $z$-direction, with a slope discontinuity at the interface, as illustrated with the solid green line in Fig. 4. The same figure also provides the values obtained at the nodes of the non-conforming mesh (circles) and the temperature value obtained right at the interface (square symbol), as provided by the IGFEM enrichments. The perfect match between the analytical and numerical results in this simple example shows that the IGFEM satisfies the patch test. illustrates the temperature profile along the $z$-axis obtained from the IGFEM solution with the non-conforming mesh shown in Fig. 5(b), for this patch test. The circular nodes depicted on this temperature profile, which is composed of two line segments, show the IGFEM solution at the FEM nodes, while the rectangular node depicts the interpolation of the temperature value at the phase interface in a nonconforming element cut by this interface. As shown there, the IGFEM provides super convergent results for this problem and yields the exact solution value along the interface in a nonconforming element.

The convergence study for the original problem is conducted using conforming structured meshes for the standard FEM, while unstructured non-conforming meshes are used for the IGFEM solutions (Fig. 5)) so that elements located across the interface are intersected along different orientations. Fig. 6 presents the convergence rates of the standard FEM and IGFEM for this problem, with respect to both the $L_2$- and $H^1$-norm of the error. As shown there, the rate of convergence of the IGFEM, without employing any corrections to the blending elements, is equivalent to that of the standard FEM. As expected, due to the simplicity of the geometry, the accuracy of the standard FEM for the same number of dofs is superior to that of the IGFEM, although the difference between the two methods is very small.

### 3.2. Example 2: Non-constant gradient jump over a curved interface

In this second example, we study the convergence rate of the IGFEM for a problem with a cylindrically shaped material interface as shown in Fig. 7(a). The cubic domain with the length of 10 cm contains a cylinder, extended along the $y$-axis, with the diameter of 7 cm and a conductivity value five times larger than that of the surrounding material. The prescribed temperature along the bottom surface of the domain is $u_b = 0\,^\circ$C while a heat flux $q = 10^5(x - 0.05) + 500$ W/m$^2$ is applied along the top surface. Both faces in the $x$ direction have conductive (Robin) boundary conditions with a heat transfer coefficient of $h = 8$ W/m$^2$ K and an ambient temperature $u_\infty = 20\,^\circ$C, while the other two surfaces are assumed to be insulated. The temperature field obtained from the IGFEM solution over the domain and in half of the matrix cut at $x$ = 5 cm are shown in Fig. 7(b) and (c), respectively.

The IGFEM and standard FEM rates of convergence of this second example are presented in Fig. 8. Since no analytical solution is available for this problem, we use a standard FEM solution with a very refined conforming mesh built on a $85 \times 85$ grid as the reference solution. As in the first example, the standard FEM solutions for this problem are obtained using conforming meshes while the unstructured non-conforming meshes similar to those shown in Fig. 5(b) are adopted for the IGFEM solution.

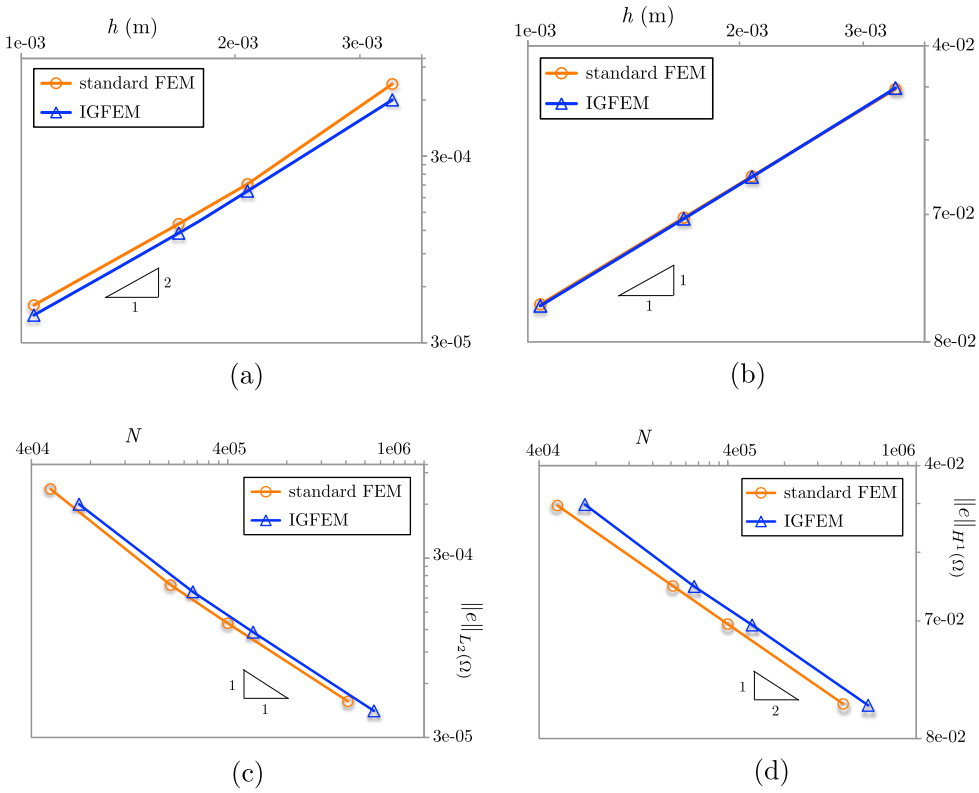


**Fig. 6.** Convergence rates in $L_2$-norm and $H^1$-norm of the error with respect to the mesh size ($h$) and total number of dofs ($N$) for the first example problem shown in Fig. 4. Conforming and nonconforming meshes similar to those presented in Fig. 5 are used for the standard FEM and IGFEM solutions, respectively.

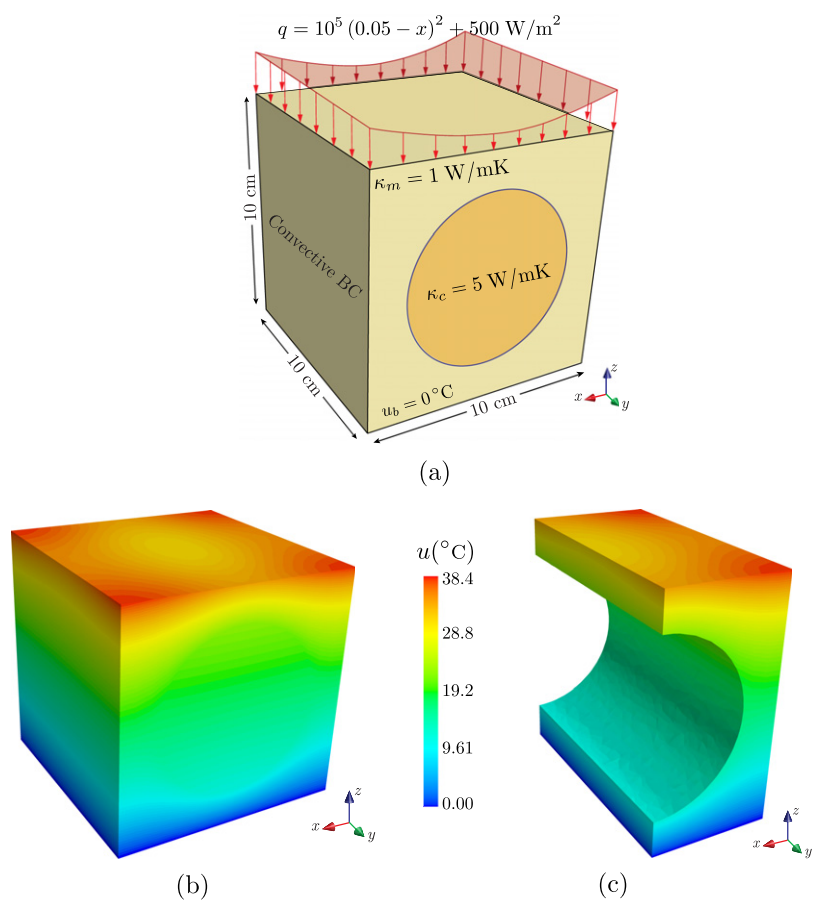


**Fig. 7.** (a) Problem description and IGFEM thermal solution over, (b) the entire domain, and (c) the matrix in half of the domain cut at $x = 5$ cm.

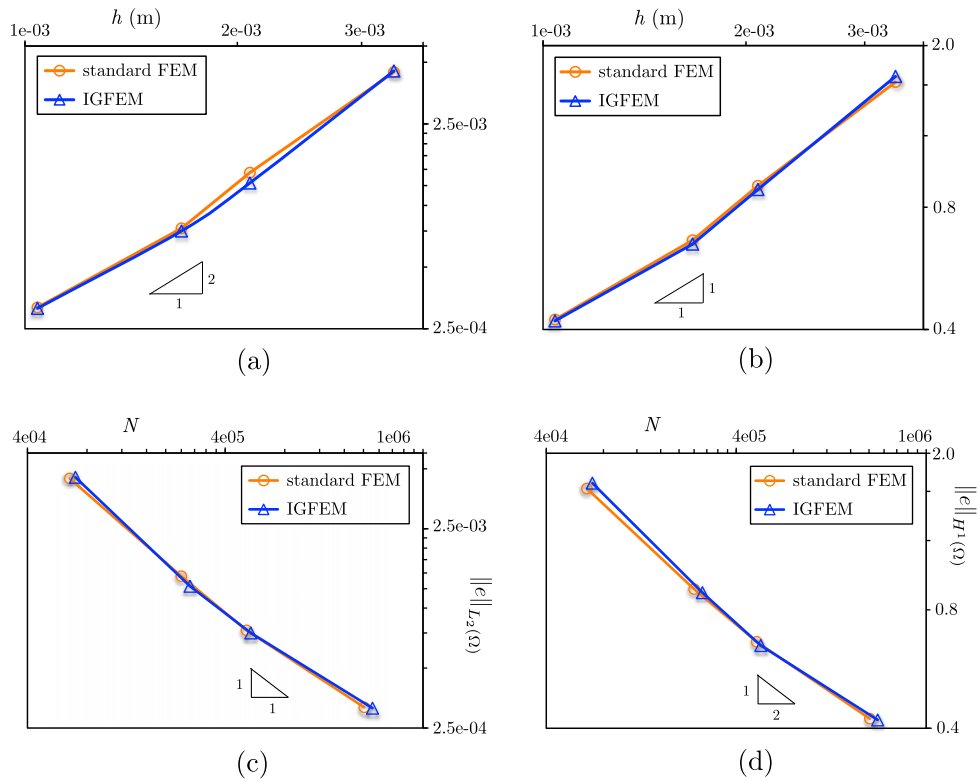


| | *h-H1* | *h-L2* | *N-H1* | *N-L2* |
|---|---|---|---|---|
| Standard FEM | 1.06 | 2.02 | 0.47 | 0.96 |
| IGFEM | 1.05 | 1.99 | 0.46 | 0.93 |

(e)

**Fig. 8.** Convergence rates in $L_2$-norm and $H^1$-norm of the error with respect to the mesh size ($h$) and number of dofs ($N$) for the second example problem described in Fig. 7. (e) presents the convergence rate values obtained from the two most refined FEM meshes for each plot.

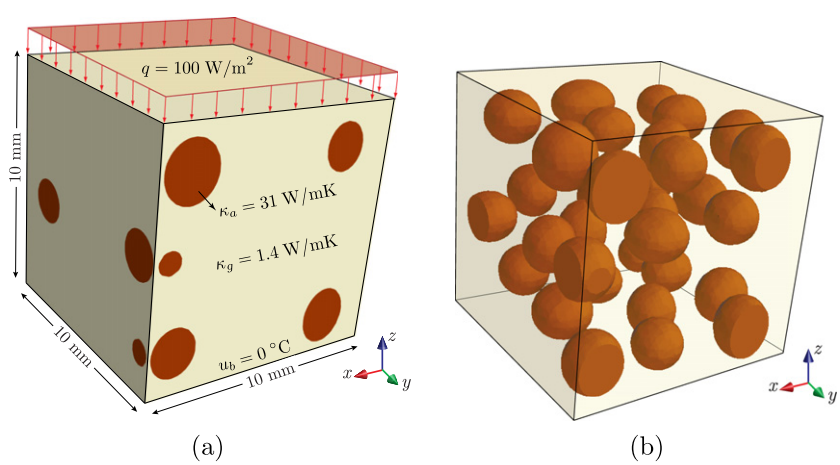


**Fig. 9.** First application problem. (a) Geometry and boundary conditions for a volume element of particulate composite with alumina inclusions embedded in a glass matrix; (b) Distribution of embedded inclusions.

As shown in Fig. 8, the IGFEM yields convergence rates similar to that of the standard FEM. Moreover, for the same number of dofs, the accuracy of the IGFEM is comparable to that of the standard FEM. It must be noted that, because of the discretization error due to the presence of the curved interface, neither the standard FEM nor the IGFEM yield the optimal rate of convergence. However, this example shows that the IGFEM achieves a performance similar to that of the standard FEM while removing the cost and complexity of creating conforming meshes.

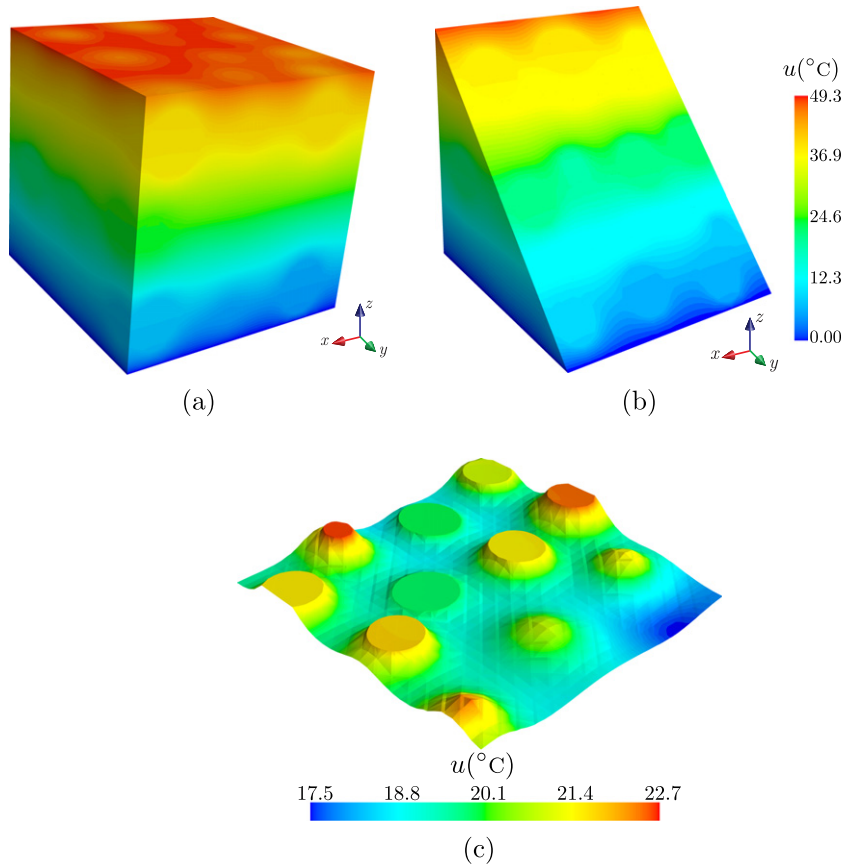


**Fig. 10.** (a) Temperature field in the first application problem presented in Fig. 9(a); (b) Temperature profile along one of the diagonal planes; (c) Temperature profile along the $z = 4$ mm plane, showing the ability of the IGFEM scheme to capture the gradient discontinuity along the particle/matrix interfaces.

## 4. Applications

The four heat transfer problems described hereafter are inspired by applications found in engineering and material science. These problems are all solved with the IGFEM, using structured meshes that do not conform to the complex microstructure or geometry of the problem.

### 4.1. Application 1: Particulate composite

In this first application, we use the IGFEM to extract the effective thermal properties of a particulate composite, composed of a glass matrix with ellipsoid alumina inclusions. As described in [34], these thermal properties depend not only on the volume fraction of the fillers, but also on the size and distribution of the inclusions. Therefore, the evaluation of the effective properties of the composite involves the solution of several configurations of the inclusions in the matrix [35]. The complexity and cost of generating conforming meshes for multiple configurations render the use of the standard FEM very labor intensive and make mesh-independent methods such as the IGFEM particularly attractive.

Fig. 9(a) illustrates the geometry and boundary conditions of a unit cell of glass/alumina composite. A prescribed temperature $u_b = 0\,^\circ\mathrm{C}$ and a uniform heat flux $q = 100\,\mathrm{W/m^2}$ compose the boundary conditions along the bottom and top surfaces, respectively, while other faces are insulated. The thermal conductivity values of the glass matrix and alumina inclusions are $\kappa_g = 1.4$ and $\kappa_a = 31\,\mathrm{W/m\,K}$, respectively. The distribution of the alumina beads in the glass matrix is presented in Fig. 9(b) where the ellipsoidal inclusions have radii ranging from 0.9 to 1.3 mm and aspect ratios between 0.75 and 1.25.

Fig. 10 illustrates the temperature field in this problem, obtained from the IGFEM solution with a non-conforming structured mesh built on a $32 \times 32 \times 32$ grid. Fig. 10(b) shows the temperature field along a diagonal place, demonstrating the heterogeneous nature of the thermal solution inside the composite. A slice of the temperature profile along the plane $z = 4$ mm is presented in Fig. 10(c), which clearly illustrates the ability of the IGFEM to cap-

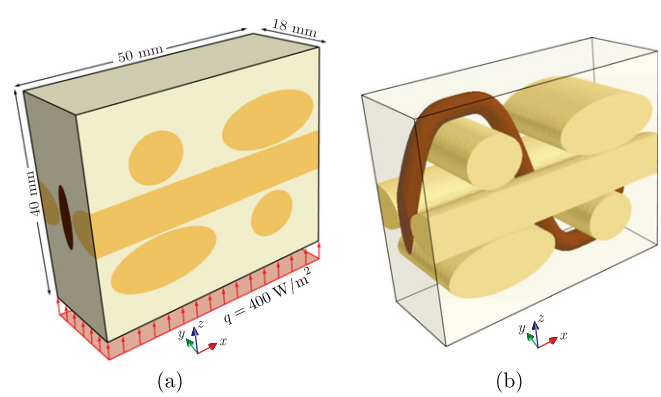


**Fig. 11.** Second application problem: (a) Geometry and applied boundary conditions of a unit cell of 3D woven composite made of epoxy matrix, glass weft and warp fiber tows, and copper z-fibers; (b) Configuration of the weft and warp tows, and of the z-fibers.

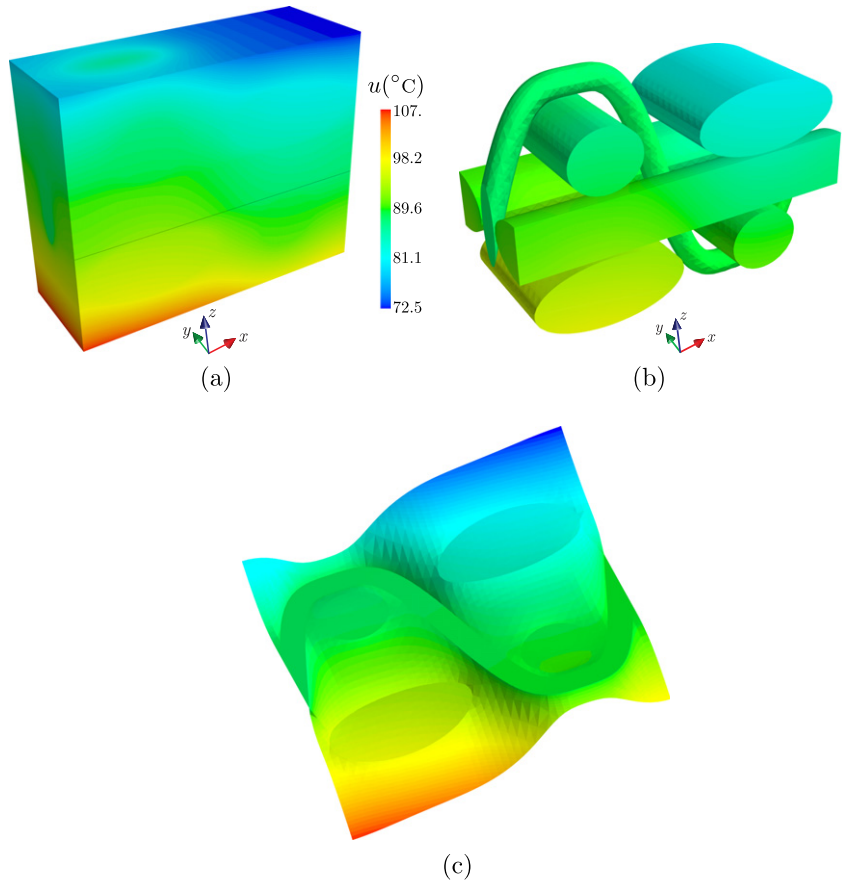


**Fig. 12.** (a) Temperature field in the second application problem described in Fig. 11; (b) Temperature solution in the glass fibers and in the copper *z*-fiber; (c) Temperature profile along $y = 9$ mm.

ture the gradient discontinuity along the perimeter of the alumina inclusions.

### 4.2. Application 2: 3D woven composites

In the second example, we use the IGFEM to evaluate the temperature field in a unit cell of a 3D woven composite inspired by the material system discussed in [36]. The dimensions, boundary conditions, and microstructure of the unit cell are shown in Fig. 11. The bottom surface of this $50 \times 18 \times 40$ mm domain is subject to a constant heat flux $q = 400$ W/m$^2$, the top surface has convective boundary conditions with $h = 7$ W/m$^2$ K and $u_\infty = 20$ °C, and other faces are insulated. The epoxy matrix holds glass fibers in the weft and warp directions, each phase with thermal conductivities of $\kappa_e = 0.3$ W/m K and $\kappa_g = 0.96$ W/m K, respectively. The z-fibers weaving together the weft and warp tows are made of copper with $\kappa_c = 401$ W/m K. A high-conductivity material for the *z*-fiber is adopted to increases the thermal conductivity of the composite in the through-thickness direction [37].

Fig. 12 illustrates the temperature field in the unit cell and in the fibers. A structured mesh built on a $50 \times 24 \times 40$ grid is used for the evaluation of the IGFEM solution for this problem. Fig. 12(b) shows the role of the copper z-fiber in transferring the heat through the thickness of the unit cell. The figure illustrates the ability of the IGFEM to capture the gradient discontinuity along the surface of the copper wire although the conductivity of the copper is more than 1300 times larger than that of the surrounding epoxy. This behavior is clearly observed in Fig. 12(c) where a slice of the temperature field is presented along the centerline of the *z*-fiber at $y = 9$ mm.

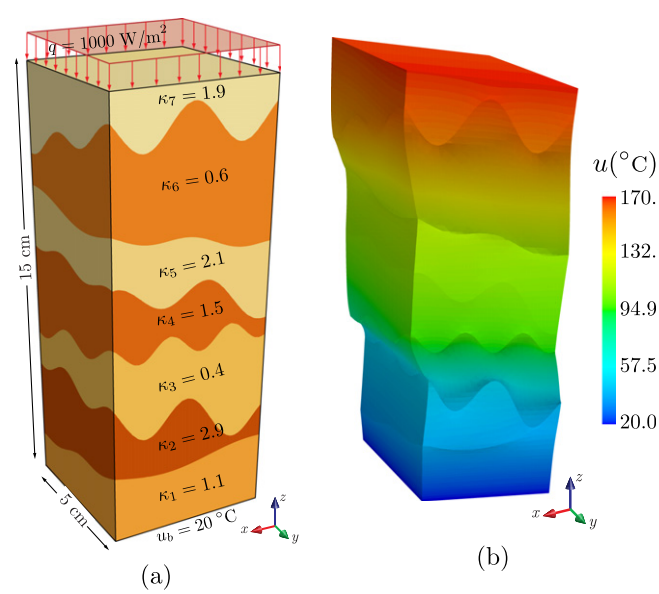


**Fig. 13.** Third application problem: (a) Geometry, boundary conditions, and material properties of a soil specimen composed of several layers where the thermal conductivity of each layers is given in W/m K; (b) Temperature field obtained with the IGFEM solver.

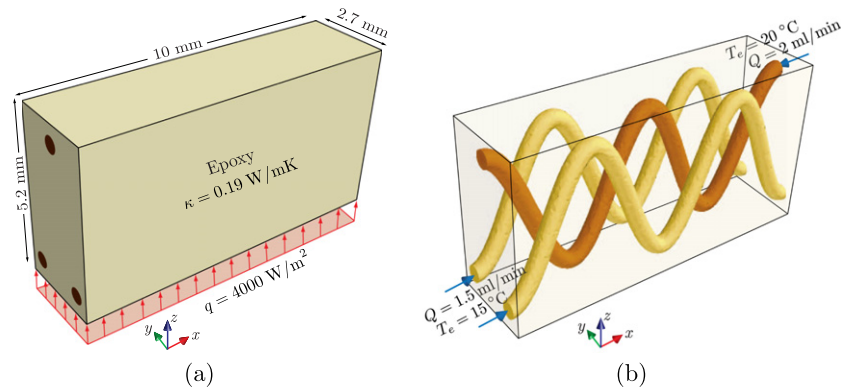


**Fig. 14.** (a) Geometry and boundary conditions for an actively-cooled epoxy fin; (b) Embedded sinusoidal-shape microchannels with the amplitude and wavelength of $A = 2$ and $\lambda = 5$ mm, respectively, and water as the coolant with flow rates and entrance temperatures specified in the figure.

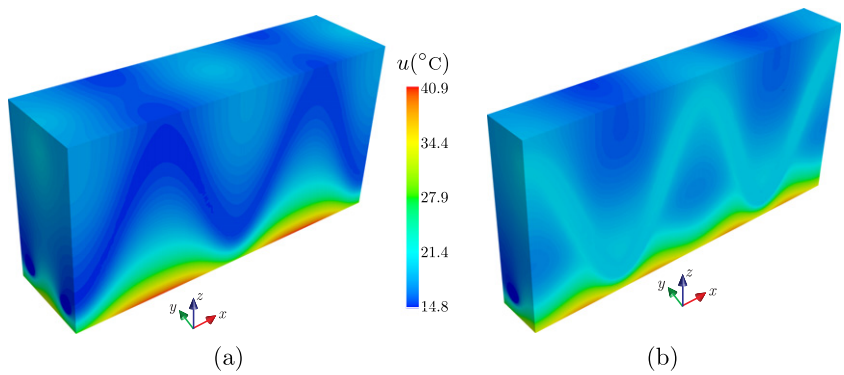


**Fig. 15.** (a) Temperature field in the microvascular epoxy fin shown in Fig. 14; (b) Temperature profile inside the domain, cut along the plane $y = 1.35$ mm, emphasizing the thermal impact of the embedded microchannels.

### 4.3. Application 3: Laminated soil

In the third application, the temperature field in a multi-layered soil sample with the dimensions shown in Fig. 13(a) is evaluated with the IGFEM. The thermal conductivity of soil is a function of several parameters such as the grain size, moisture content, density, porosity, and organic matter and thus could be considerably different from one layer to the next [38]. The temperature of the specimen is fixed at $u_b = 20\,^\circ$C along the bottom surface of the specimen and a constant heat flux with intensity $q = 1000$ W/m K is applied along the top boundary, while other faces are kept insulated. The IGFEM solution obtained with a $25 \times 25 \times 75$ structured mesh is presented in Fig. 13(b). The temperature field is slightly warped in both the $x$ and $y$ directions to emphasize the discontinuity in the gradient field across the interfaces between different layers.

### 4.4. Application 4: Actively-cooled microvascular polymeric fin

Microvascular materials are being considered for various engineering applications such as autonomic materials [39,40], biotechnology [41,42], and microelectromechanical systems (MEMS) [43–45]. In such materials, the diameter of the embedded microchannels varies from a few microns to a millimeter, and the embedded network of microchannels is designed based on a variety of application-driven objective functions (thermal impact, flow efficiency, mechanical impact, ...) and manufacturing constraints. In this last example problem, we employ the IGFEM to evaluate the temperature field in an actively-cooled microvascular epoxy fin [46–48]. The specimen dimensions, applied thermal boundary conditions, and configuration of the microchannels are shown in Fig. 14. The $10 \times 2.7 \times 5.2$ mm epoxy fin with $\kappa = 0.19$ W/m K is subject to a constant heat flux $q = 4000$ W/m$^2$ along the bottom surface and convective boundary condition with $h = 7$ W/m K and $u_\infty = 20\,^\circ$C along the other surfaces.

Fig. 14(b) illustrates the configuration of the embedded microchannels in the epoxy matrix with diameters $D = 500\ \mu$m. A sinusoidal-shaped curve with the amplitude $A = 2$ mm and wavelength $\lambda = 5$ mm describes the centerline of the microchannels. The coolant circulating in the channels is water with $\kappa_w = 0.6$ W/m K, $\rho = 1000$ kg/m$^3$, and $c_p = 4185.5$ J/kg K. The middle channel carries a flow rate of $Q = 2$ ml/min with the entrance temperature $T_e = 20\,^\circ$C while the two other microchannels have a slightly smaller flow rate, $Q = 1.5$ ml/min, with $T_e = 15\,^\circ$C in the opposite direction.

The evaluation of the convection term in (1) associated with the fluid flow requires the knowledge of the velocity field in the microchannels. Due to the very small size of microchannels and the small value of the mass flow rate, laminar flow condition with fully-developed velocity profile adequately describes the flow in the channels. The magnitude of the velocity in the flow direction at a distance $r$ from the centerline of the microchannel is then expressed as [49]:

$$|\mathbf{v}| = 1.5\overline{v}\left(1 - \frac{4r^2}{D^2}\right),$$

where $\overline{v}$ is the mean velocity in the channel.

The IGFEM solution for this problem is presented in Fig. 15. From Fig. 15a, which shows the temperature field along three of the outer surfaces of the domain, the thermal impact of the coolant circulating in the three microchannels is clearly observable. Fig. 15c presents details of the temperature field inside the domain along the vertical plane $y = 1.35$ mm (at the centerline of the middle channel), depicting the jump in the gradient field along the surface of the microchannel due to the mismatch in the thermal conductivity values.

## 5. Conclusions

An interface-enriched generalized finite element formulation has been introduced to solve 3D problems characterized by discontinuous gradient fields. In this method, the generalized degrees of freedom introduce to enrich the numerical solution in non-conforming elements traversed by a material interface are associated with the interface nodes, and not with the nodes of the non-conforming mesh as in conventional GFEM. This choice leads to some implementation advantages such as the straightforward handling of Dirichlet boundary conditions. Moreover, the number of the generalized dofs associated with the IGFEM, which determines the computational cost of the method, is similar to that of conventional GFEM in the absence of blending elements. The enrichment functions for the IGFEM consist in a linear combination of the Lagrangian shape functions defined on the integration elements. In this work, the enrichment functions for four-node tetrahedral elements have been derived. It was also pointed out how the IGFEM is able to handle more complex cases such as the presence of multiple interfaces in a given element. The flexibility of the IGFEM for evaluating the enrichment functions makes this approach highly suited for problems with intricate internal geometries.

A detailed convergence study of the IGFEM for 3D heat transfer problems with straight and curved interfaces has also been conducted, showing that the IGFEM yields similar rate of convergence and accuracy level with non-conforming meshes as that of the standard FEM with conforming meshes. Thermal problems in heterogeneous materials and structures ranging from composites to microvascular polymer have been investigated to demonstrate the flexibility of the IGFEM in capturing weakly discontinuous solutions in a variety of complex internal geometries.

## 6. Acknowlegment

This work has been supported by the Air Force Office of Scientific Research Multidisciplinary University Research Initiative (Grant No. FA9550-09-1-0686). The authors also wish to thank insightful discussions with Prof. C. A. Duarte at the University of Illinois.

## References

[1] C.A. Duarte, T.J. Oden, H-p clouds - an h-p meshless method, Numer. Methods Partial Diff. Eqs. 12 (6) (1996) 673–705.
[2] T.J. Oden, C.A. Duarte, O.C. Zienkiewicz, A new cloud-based hp finite element method, Comput. Methods Appl. Mech. Engrg. 153 (1-2) (1998) 117–126.
[3] J.M. Melnek, I. Babuska, The partition of unity finite element method: Basic theory and applications, Comput. Methods Appl. Mech. Engrg. 139 (1-4) (1996) 289–314.
[4] I. Babuska, J.M. Melnek, The partition of unity method, Int. J. Numer. Methods Engrg. 40 (4) (1997) 727–758.
[5] T. Belytschko, T. Black, Elastic crack growth in finite elements with minimal remeshing, Int. J. Numer. Methods Engrg. 45 (5) (1999) 601–620.
[6] N. Moës, J. Dolbow, T. Belytschko, A finite element method for crack growth without remeshing, Int. J. Numer. Methods Engrg. 46 (1) (1999) 131–150.
[7] C.A. Duarte, I. Babuška, T.J. Oden, Generalized finite element methods for three-dimensional structural mechanics, Comput. Struct. 77 (2) (2000) 215–232.
[8] N. Sukumar, N. Moës, B. Moran, T. Belytschko, Extended finite element method for three-dimensional crack modeling, Int. J. Numer. Methods Engrg. 48 (2000) 1549–1570.
[9] N. Moës, T. Belytschko, Extended finite element method for cohesive crack growth, Engrg. Fracture Mech. 69 (2002) 813–833.
[10] J.H. Song, P.M.A. Areias, T. Belytschko, A method for dynamic and shear band propagation with phantom nodes, Int. J. Numer. Methods Engrg. 67 (2006) 868–893.
[11] J. Fish, Z. Yuan, Multiscale enrichment based on partition of unity, Int. J. Numer. Methods Engrg. 62 (2005) 1341–1359.
[12] J. Dolbow, N. Moës, T. Belytschko, Discontinuous enrichment in finite elements with a partition of unity method, Finite Elements Anal. Desig. 36 (2000) 235–260.
[13] A.R. Khoei, M. Nikbakht, Contact friction modeling with the extended finite element method (X-FEM), J. Mat. Sci. Technol. 177 (2006) 58–62.
[14] J. Chessa, T. Belytschko, An enriched finite element method and level sets for axisymetric two-phase flow with surface tension, Int. J. Numer. Methods Engrg. 58 (2003) 2041–2064.
[15] R. Gracie, G. Ventura, T. Belytschko, A new fast method for dislocations based on interior discontinuities, Int. J. Numer. Methods Engrg. 69 (2007) 423–441.
[16] J. Oswald, R. Gracie, R. Khare, T. Belytschko, An extended finite element method for dislocations in complex geometries: thin films and nanotubes, Comput. Methods Appl. Mech. Engrg. 198 (2009) 1872–1886.
[17] A.M. Aragón, C.A. Duarte, P.H. Geubelle, Generalized finite element enrichment functions generalized finite element enrichment functions for discontinuous gradient fields, Int. J. Numer. Methods Engrg. 82 (2010) 242–268.
[18] N. Sukumar, Z. Hang, J.H. Prevost, Z. Suo, Partition of unity enrichment for bimaterial interface cracks, Int. J. Numer. Methods Engrg. 59 (2004) 1075–1102.
[19] N. Moës, M. Cloirec, P. Cartraud, J.F. Remacle, A computational approach to handle complex microstructure geometries, Comput. Methods Appl. Mech. Engrg. 192 (2003) 3163–3177.
[20] T. Belytschko, R. Gracie, G. Ventura, A review of extended generalized finite element methods for material modeling, Model. Simul. Mat. Sci. Eng. 17 (2009) 043001.
[21] J.C. Michel, H. Moulinec, P. Suquet, Effective properties of composite materials with periodic microstructure: a computational approach, Comput. Methods Appl. Mech. Engrg. 16 (1999) 109–143.
[22] Y.S. Song, J.R. Youn, Evaluation of effective thermal conductivity for carbon nanotube/polymer composites using control volume finite element method, Carbon 44 (4) (2006) 710–717.
[23] X.F. Wang, G.M. Zhou, X.W. Wang, C.W. Zhou, Multi-scale analyses of 3D woven composite based on periodicity boundary conditions, J. Composite Mat. 41 (14) (2007) 1773–1788.
[24] C. Miehe, J. Schroder, J. Schotte, Computational homogenization analysis in finite plasticity simulation of texture development in polycrystalline materials, Comput. Methods Appl. Mech. Engrg. 9 (1999) 387–418.
[25] M. Iuga, F. Raether, FEM simulations of microstructure effects on thermoelastic properties of sintered ceramics, J. Eur. Ceramic Soc. 27 (2007) 511–516.
[26] U.M. Mayer, A. Popp, A. Gerstenberger, W.A. Wall, 3d fluid-structure-contact interaction based on a combined xfem fsi and dual mortar contact approach, Comput. Mech. 46 (2010) 53–67.
[27] L.A. Shipton, Thermal management applications for microvascular systems, Master's thesis, University of Illinois at Urbana-Champaign, 2007.
[28] F. Armero, C. Linder, New finite element methods with embedded strong discontinuities in the finite deformation range, Comput. Methods Appl. Mech. Engrg. 197 (2008) 3138–3170.
[29] O.C. Zienkiewicz, R.L. Taylor, J.Z. Zhu, The Finite Element Method: Its Basis and Fundamentals, Elsevier, 2005.
[30] S. Soghrati, A.M. Aragón, C.A. Duarte, P.H. Geubelle, An interface-based generalized finite element method for problems with discontinuous gradient fields, Int. J. Numer. Methods Engrg., in press, doi:10.1002/nme.3273.
[31] T.P. Fries, A corrected XFEM approximation without problems in blending elements, Int. J. Numer. Methods Engrg. 75 (5) (2008) 503–532.
[32] N. Moës, E. Béchet, M. Tourbier, Imposing Dirichlet boundary conditions in the extended finite element method, Int. J. Numer. Methods Engrg. 67 (12) (2006) 1641–1669.
[33] I. Babuska, U. Banerjee, J.E. Osborn, Survey of meshless and generalized finite element methods: a unified approach, Acta Numerica 12 (2003) 1–125.
[34] N. Tessier-Doyen, X. Grenier, M. Huger, D.S. Smith, D. Fournier, J.P. Roger, Thermal conductivity of alumina inclusion/glass matrix composite materials: local and macroscopic scales, J. Eur. Ceramic Soc. 27 (2007) 2635–2640.
[35] J. Floury, J. Carson, Q.T. Pham, Modeling thermal conductivity in heterogeneous media with finite element method, Food Bioprocess Technol. 1 (2008) 161–170.
[36] L. Tong, A.P. Mouritz, M.K. Bannister, 3D Fibre Reinforced Polymer Composites, Elsevier, 2002.
[37] A.E. Bogdanivich, M.H. Mohamad, Three-dimensional reinforcements for composites, SAMPE J. 45 (6) (2009) 8–28.
[38] N.H. Abu-Hamdeh, R. Reeder, Soil temperature conductivity: effect of density, moisture, salt concentration, and organic matter, Soil Sci. Soc. Am. J. 64 (2000) 1285–1290.
[39] S.R. White, N.R. Sottos, P.H. Geubelle, J.S. Moore, M.R. Kessler, S.R. Sriram, E.N. Brown, S. Viswanathan, Autonomic healing of polymer composites, Nature 409 (2001) 794–797.

[40] D. Therriault, S.R. White, J.A. Lewis, Chaotic mixing in three-dimensional microvascular networks fabricated by direct-write assembly, Nature Mat. 2 (2003) 256–271.
[41] M.A. Burns, B.N. Johnson, S.N. Brahmasandra, K. Handique, J.R. Webster, M. Krishnan, T.S. Sammarco, P.M. Man, D.JonesD. Heldsinger, C.H. Mastrangelo, D.T. Burke, An integrated nanoliter dna analysis device, Science 282 (1998) 484–487.
[42] A. Strömberg, A. Karlsson, F. Ryttsén, M. Davidson, D.T. Chiu, O. Orwar, Microfluidic device for combinatorial fusion of liposomes and cells, Anal. Chem. 73 (2001) 126–130.
[43] Y. Wang, G. Yuan, Y.K. Yoon, M.G. Allen, S.A. Bidstrup, Active cooling substrates for thermal management of microelectronics, IEEE Trans. Components Packaging Technol. 28 (3) (2005) 477–483.
[44] R.B. Oueslati, D. Therriault, S. Martel, Pcb-integrated heat exchanger for cooling electronics using microchannels fabricated with the direct-write method, IEEE Trans. Components Packaging Technol. 31 (4) (2008) 869–874.
[45] V.G. Pastukhov, Y.F. Maidanik, C.V. Vershinin, M.A. Korukov, Miniature loop heat pipes for electronics cooling miniature loop heat pipes for electronics cooling miniature loop heat pipes for electronics cooling, Appl. Therm. Engrg. 23 (9) (2003) 1125–1135.
[46] K.S. Toohey, N.R. Sottos, J.A. Lewis, J.S. Moore, S.R. White, Self-healing materials with microvascular networks, Nature Mat. 6 (2007) 581–585.
[47] A.M. Aragón, J.K. Wayer, P.H. Geubelle, D.E. Goldberg, S.R. White, Design of microvascular flow networks using multi-objective genetic algorithms, Comput. Methods Appl. Mech. Engrg. 197 (2008) 4399–4410.
[48] S.C. Olugebefola, A.M. Aragón, C.J. Hansen, A.R. Hamilton, B.D. Kozola, W. Wu, P.H. Geubelle, J.A. Lewis, N.R. Sottos, S.R. White, Polymer microvascular network composite, J. Composite Mat. 44 (22) (2010).
[49] C.A. Brebbia, A. Ferrante, Computational Hydraulics, Butterworth, 1983.